# 4.0 MODELING DIFFRACTION IN THE MONTE-CARLO RAY-TRACE ENVIRONMENT

In the Theory of Heat Radiation, Max Plank [1959] states that "so far as their physical properties are concerned, heat rays are identical with light rays of the same wavelength". His book, which contains much of the basis upon which modern radiation heat transfer is based, does not consider the phenomenon of diffraction "on account of its complicated nature". Plank goes on to say "[i]t will be assumed that the linear dimensions of all parts of space considered, as well as the radii of curvature of all surfaces under consideration, are large compared with the wavelengths of the rays considered. With this assumption we may, without appreciable error, entirely neglect the influence of diffraction caused by the bounding surfaces, and everywhere apply the ordinary laws of reflection and refraction of light". Many of the instruments modeled by the Thermal Radiation Group do not adhere to this restriction, rather some of the instrument dimensions are on the order of the wavelength of the entering radiation. In such cases, general methods used to model radiation heat transfer must be supplemented with some means of dealing with diffraction in the development of the complete radiative model of an instrument.

Much of the work done in the Thermal Radiation Group involves the development of radiative models of instruments using the Monte-Carlo ray-trace (MCRT) method. This

is a statistical approach which simulates the behavior of radiant energy as it enters and passes through an instrument. A complete description of this method can be found in Walkup [1996]. To model radiant energy as it enters an instrument in the MCRT environment, the entering energy is divided into a large number of discrete energy bundles. These bundles are fired uniformly and randomly into the aperture. For example, for the case of a rectangular aperture with corner coordinates of $(X_o,Y_o)$ and width and length (W,L), illustrated in Figure 4.1, a given energy bundle will enter at location $X=X_o+R_xL$, $Y=Y_o+R_yW$, where $R_x$ and $R_y$ are random numbers uniformly distributed between 0 and 1. Up to this point, radiative models created in the Thermal Radiation Group ignored diffraction effects and the entering energy bundles were directed parallel into the instrument and treated as collimated energy. It is desirable to develop a means of modeling the true behavior of this radiation as it enters and passes through the instrument. This proper modeling of the diffraction of radiant energy as it enters radiometric instruments is addressed in this chapter by presenting two candidate modeling approaches.

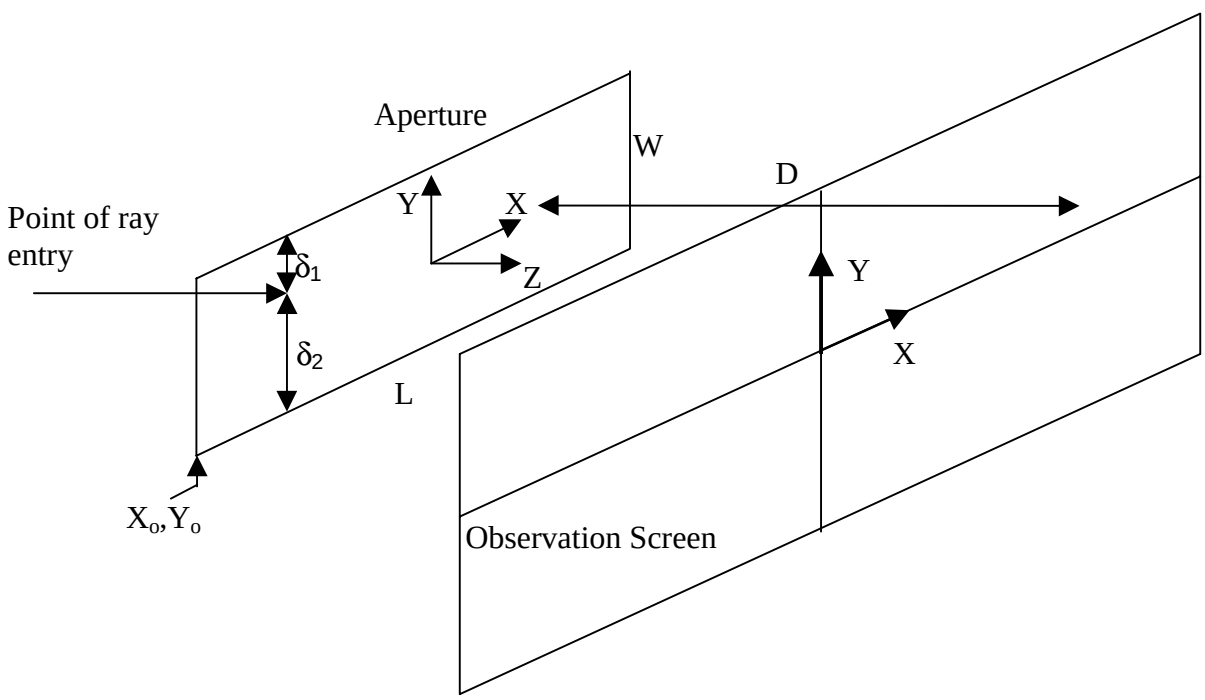


**Figure 4.1** Illustration of physical parameters important to the description of the statistical model of diffraction.

## 4.1 Model 1: The statistical approach

The statistical approach to modeling diffraction was originally published by Heinisch and Chou [1971], and later modified and republished by Likeness [1977]. This approach treats diffraction of energy as it enters through an aperture in a statistical manner, and is designed for application in the Monte-Carlo ray-trace environment. It is based on Heisenberg's uncertainty principle and the particle theory of light. Neither of the two references that describe this approach includes many details of its implementation. The details necessary to successfully implement this approach, as developed by the current author are presented. Note that these details may differ from those used by the original developers of this method.

### 4.1.1 Appropriate application of the statistical approach

Rays are directed into the aperture as appropriate in the Monte-Carlo environment, and the distances $\delta_1$ and $\delta_2$ from the point of entry to the aperture edges are calculated for each entering ray, as illustrated in Figure 4.1. Experience tells us that entering rays will be diffracted; however, the extent to which this diffraction occurs depends upon the wavelength of the entering radiation relative to the dimensions of the aperture through which it enters. When modeling the diffraction of rays as they pass through an aperture which is much larger than the wavelength of the entering radiation, only rays in a limited region, or no rays at all, should be diffracted. In some such cases it will be acceptable to neglect diffraction altogether and use an ideal ray approximation. Wyatt [1987] suggests that this approximation is only acceptable when $\Delta\xi > 10.0$ (where $\Delta\xi$ is given by equation 3.1). However, diffraction patterns shown in Figure 3.4 indicate that this rule may be too restrictive. Regardless, when modeling a case in which the entering wavelength is much shorter than the dimensions of the aperture through which it enters, but where the ideal ray approximation would not be appropriate, Likeness [1977] suggests that the statistical diffraction model be applied to within $50\lambda$ to $500\lambda$ from the edge, while Morbey and Hutchings [1993] suggest application to within $100\lambda$.

If the dimensions of the aperture are on the order of the wavelength of the entering energy, all entering rays must be diffracted. The statistical approach treats diffraction as

an edge effect, and the question arises as to which edge (or if both edges) of the aperture should affect the entering energy bundle. A method of dealing with such cases appropriately is needed. Four methods were investigated and are presented in this chapter. However from this point forward, the parameter $\delta$ is used as a general parameter that takes on both values, $\delta_1$ and $\delta_2$, depending on the ray that is being traced and the method being used.

### 4.1.2 Description of the statistical approach

This approach is based in part on the Heisenburg uncertainty principle, which states that when making simultaneous measurements of a particle's momentum, p, and position, x, the product of the uncertainties in these two measurements cannot be less than $\frac{\hbar}{2}$, where $\hbar = \frac{h}{2\pi}$, and h is Planck's constant ($6.63 \times 10^{-34}$ J•s).

That is,

$$\Delta p \times \Delta x \geq \frac{\hbar}{2}, \tag{4.1}$$

where $\Delta$ indicates the amount of uncertainty in a particular measurement. Since a particle's position is described in three dimensions, we can write the uncertainty principle in three ways:

$$\Delta p_x \times \Delta x \geq \frac{\hbar}{2}, \tag{4.2}$$

$$\Delta p_y \times \Delta y \geq \frac{\hbar}{2}, \tag{4.3}$$

and

$$\Delta p_z \times \Delta z \geq \frac{\hbar}{2}. \tag{4.4}$$

We model Heisenburg's uncertainty principle as an equality,

$$\Delta p_y \times \Delta y = \frac{\hbar}{2} = \frac{h}{4\pi}, \tag{4.5}$$

and take the uncertainty in position (in the y direction) of an entering energy bundle to be $\delta$, the distance from the point of entry to the aperture edge. Thus

$$\Delta p_y = \frac{h}{4\delta\pi}. \tag{4.6}$$

Referring to the construction of Figure 4.2, the uncertainty in momentum in the y direction is interpreted in terms of an angle of diffraction. We define $\phi^*$ as the maximum angle of diffraction where the angle of diffraction, $\phi_d$, is less than or equal to $\pm\,\phi^*$. Thus $\phi^*$ defines the range of values that $\phi_d$ can take on.

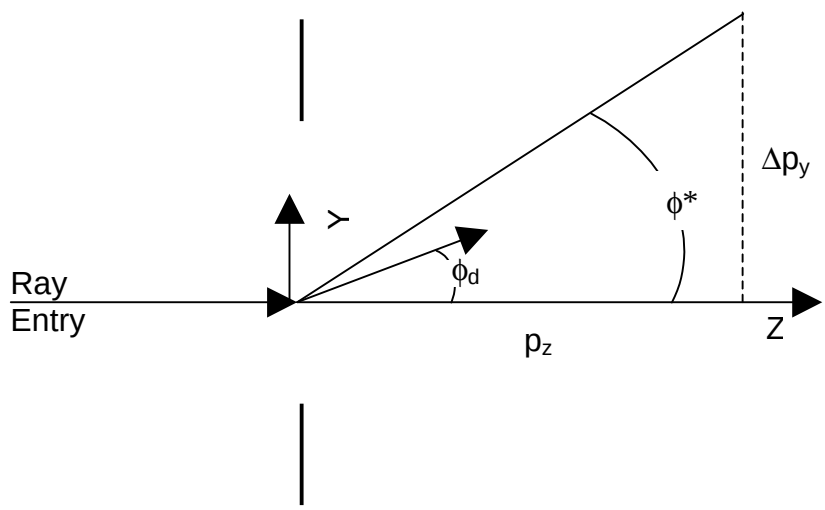


**Figure 4.2** Illustration of possible spread of diffraction angles in the application of the statistical approach to modeling diffraction.

Using this construction we can write

$$\tan(\phi^*) = \frac{\Delta p_y}{p_z}. \tag{4.7}$$

Using the equalities $p_z = \frac{h}{\lambda}$, the wave number, $k = \frac{2\pi}{\lambda}$, and equation 4.6, and substituting into equation 4.7 yields

$$\tan(\phi^*) = \frac{\Delta p_y}{p_z} = \frac{1}{2k\delta}, \tag{4.8}$$

or

$$\phi^* = \tan^{-1}\left(\frac{1}{2k\delta}\right). \tag{4.9}$$

Likeness proposed the use of a normal distribution as the probability density function of the diffracted energy, where the most probable path of an entering energy bundle is straight ahead (mean, $\mu$=0), and the standard deviation is taken to be $\phi^* = \tan^{-1}\left(\frac{1}{2k\delta}\right)$.

Thus

$$p(\phi_d) = \frac{1}{\sqrt{2\pi}\ \phi^*} \exp\left[-\frac{1}{2}\left(\frac{\phi_d}{\phi^*}\right)^2\right]; \qquad (-\infty \le \phi_d \le \infty) \qquad (4.10)$$

is the probability that a ray will be diffracted at an angle $\phi_d$ from its original line of travel due to the influence of a single aperture edge. In order to make use of this probability density function in a Monte-Carlo ray-trace environment, we integrate the probability density function with respect to $\phi_d$ from $-\infty$ to $\phi_d$ to obtain the cumulative distribution function (c.d.f). A c.d.f., $P_x(x)$, has the useful property that "if x is a random number, and we have the c.d.f, $P_x(x)$, and if $P_x(x)$ is continuous, the random variable Y produced by the transformation $Y=P_x(x)$ has a uniform distribution over the interval (0,1)" [Gibbons and Chakraborti, 1992]. For a more detailed discussion of this c.d.f. property, see Walkup [1996]. We must interpret this integral in terms of the physical limits, where the range of angles that $\phi_d$ can subtend after entering the aperture is limited to $\left(-\frac{\pi}{2} \le \phi_d \le \frac{\pi}{2}\right)$, as illustrated in Figure 4.3.

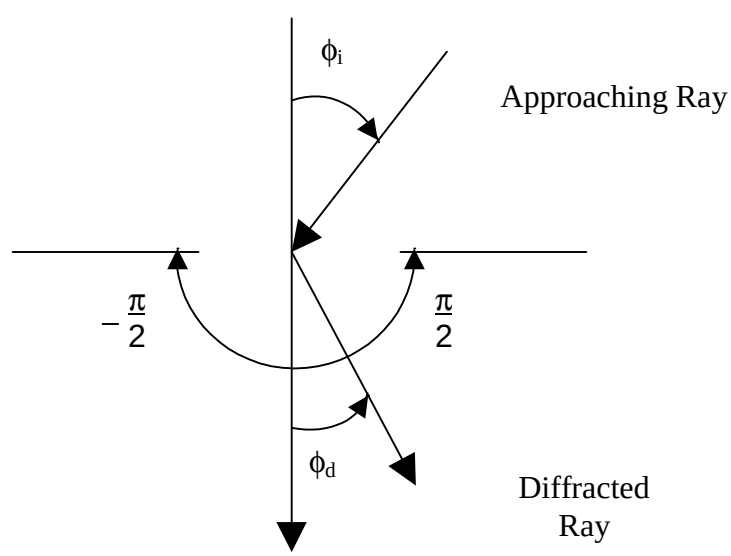


**Figure 4.3** Illustration of approaching and diffracted ray angles.

We must therefore do a substitution such that when $|\phi_d| \geq \frac{\pi}{2}$, $p(\phi_d) = 0$. Such is the case when evaluating $p(\tan(\phi_d))$ as illustrated in Figure 4.4.

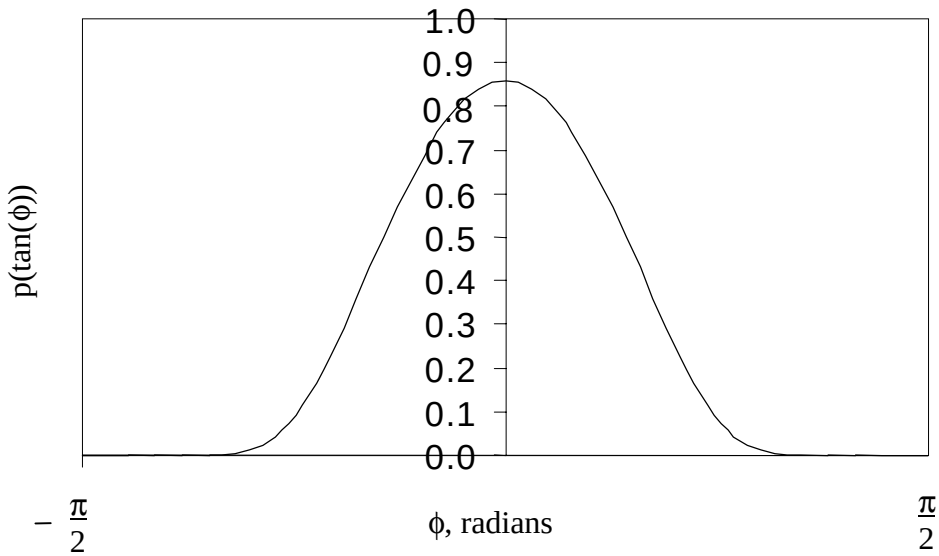


**Figure 4.4** Probability density function of $\tan(\phi_d)$

The c.d.f., which ranges uniformly between (0-1), becomes

$$P[\tan(\phi_d)] = \int_{\phi'_d=-\infty}^{\phi_d} p(\tan\phi'_d)\ d(\tan\phi'_d) = \text{Random number uniformly distributed} \tag{4.11}$$

between 0 and 1, where

$$p[\tan(\phi'_d)] = \frac{1}{\sqrt{2\pi}\ \phi^*} \exp\left[-\frac{1}{2}\left(\frac{\tan(\phi'_d)}{\phi^*}\right)^2\right]. \tag{4.12}$$

Thus

$$P[\tan(\phi_d)] = \frac{1}{\sqrt{2\pi}\ \phi^*} \int_{-\infty}^{\phi_d} \exp\left[-\frac{1}{2}\left(\frac{\tan(\phi'_d)}{\phi^*}\right)^2\right] d(\tan(\phi'_d)\,. \tag{4.13}$$

Making the substitution

$$a^2 = \frac{1}{2\ (\phi^*)^2},\ a = \frac{1}{\sqrt{2}\ \phi^*},$$

there results

$$P[\tan(\phi_d)] = \frac{1}{\sqrt{2\pi}\ \phi^*} \int_{-\infty}^{\phi_d} \exp\left[-a^2 \tan^2(\phi'_d)\right] d[\tan(\phi'_d)]. \tag{4.14}$$

A second substitution, $u = a\tan(\phi'_d)$, thus $du = ad[\tan(\phi'_d)]$ yields

$$P[\tan(\phi_d)] = \frac{1}{\sqrt{2\pi}\ \phi^*} \int_{-\infty}^{a(\tan\phi_d)} \exp\left(-u^2\right)\frac{du}{a} = R_\phi, \tag{4.15}$$

where $R_\phi$ is a random number uniformly distributed between 0 and 1. Rearranging and multiplying both sides of equation 4.15 by 2, there results

$$2\sqrt{2}\ \phi^* a\, R_\phi = \frac{2}{\sqrt{\pi}} \int_{-\infty}^{a(\tan\phi_d)} \exp(-u^2)\ du. \tag{4.16}$$

Substituting $a = \frac{1}{\sqrt{2}\ \phi^*}$ on the left-hand side yields

$$2R_\phi = \frac{2}{\sqrt{\pi}} \int_{-\infty}^{a(\tan\phi_d)} \exp(-u^2)\ du. \tag{4.17}$$

Equation 4.17 can be rewritten

$$2R_\phi = \frac{2}{\sqrt{\pi}} \int_{-\infty}^{0} \exp(-u^2)\ du + \frac{2}{\sqrt{\pi}} \int_{0}^{a(\tan\phi_d)} \exp(-u^2)\ du \tag{4.18}$$

or

$$2R_\phi = -\frac{2}{\sqrt{\pi}} \int_{0}^{-\infty} \exp(-u^2)\ du + \frac{2}{\sqrt{\pi}} \int_{0}^{a(\tan\phi_d)} \exp(-u^2)\ du. \tag{4.19}$$

Then invoking the definition and properties of the error function,

$$\mathrm{erf}(x) \equiv \frac{2}{\sqrt{\pi}} \int_0^x \exp(-\eta^2)\ d\eta,\ \mathrm{erf}(-x) = -\mathrm{erf}(x),\ \mathrm{erf}(\infty) = 1,\ \mathrm{erf}(0) = 0,$$

we find that

$$2R_\phi = -\mathrm{erf}(-\infty) + \mathrm{erf}\left[a\tan(\phi_d)\right] = 1 + \mathrm{erf}\left[a\tan(\phi_d)\right]. \tag{4.20}$$

Finally, substituting $a = \frac{1}{\sqrt{2}\ \phi^*}$ yields

$$2R_\phi - 1 = \mathrm{erf}\left(\frac{\tan(\phi_d)}{\sqrt{2}\ \phi^*}\right). \tag{4.21}$$

Equation 4.21 is used to determine the angle at which the entering ray is diffracted. An additional programming step may be required in order to arrive at a value for $\phi_d$. If using a programming language without a built-in error function (such as FORTRAN), an infinite series approximating the error function and the root-finding bisection method can be used to find the value of x when erf(x) is known. This infinite series, given by

$$\mathrm{erf}(x) = \frac{2}{\sqrt{\pi}}\left(x - \frac{x^3}{3\cdot 1!} + \frac{x^5}{5\cdot 2!} - \frac{x^7}{7\cdot 3!} + \ldots\right), \tag{4.22}$$

when expanded to eleven terms approximates the error function quite well when erf(x) ≤ 0.992869. Additional terms do not provide much improvement, as shown in Figure 4.5. If erf(x) is between 0.992869 and 1, this infinite series deviates from erf(x), and x can be approximated as 2 (or any other number greater than 2). The subroutine used is provided in Appendix A. Note that the results obtained using this subroutine were compared to results found using FORTRAN Powerstation, which includes a built-in error function. The resulting diffraction patterns were identical, thus it can be concluded that either the necessary approximations had no effect on the results, or that FORTRAN Powerstation makes the same approximations.

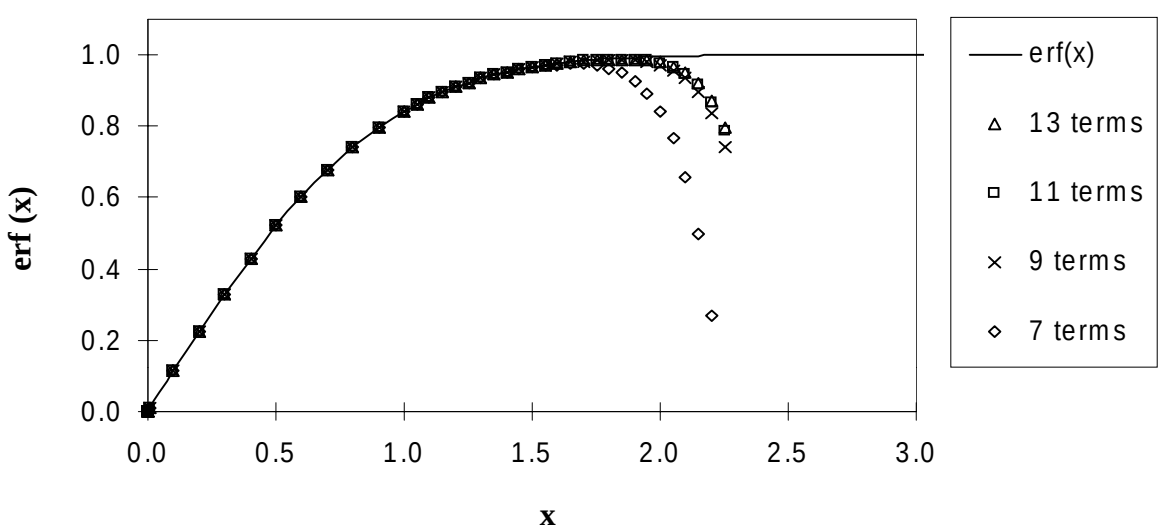


**Figure 4.5** Approximating the error function with an infinite series with an increasing number of terms.

### 4.1.3 Determining the diffraction pattern

As previously noted, for cases in which the wavelength of the entering radiation is of the same order as the dimensions of the aperture through which rays enter, each entering ray must be diffracted in some way. The angle of diffraction depends on the method chosen and the point of ray entry. After being diffracted in some way, the energy bundle continues until it is intercepted by the observation screen, and this point of interception is determined. In order to keep track of the spatial distribution of rays as they arrive at the observation screen illustrated in Figure 4.1, the screen is divided into a large number of strips in the y direction, serving as discrete "bins". Each time that a diffracted ray arrives at one of these bins, a counter is incremented for that particular bin. This provides the distribution of diffracted energy along the y direction. The number of rays arriving in each bin is normalized with respect to the bin with the most arriving rays. This normalized curve is then scaled such that the area beneath the resulting curve is approximately the same as that beneath the curve of the analytical solution (here this has been done "by eye"). This was similar to the approach used by Heinsch and Chou [1971], as they report using a scaling factor, f, which is determined by trial and error to give the best possible match with the analytical solution. The statistical approach does not keep track of phase, thus the results obtained do not model the side fringes of the analytical interference pattern, rather they form a single smooth curve that averages these fringes. Keeping track of phase would not result in a diffraction pattern with the details of the side fringes, for reasons that will become clear after the presentation of the second model. These results are adequate for most modeling efforts as it will usually suffice to know the approximate distribution of diffracted energy, which can be modeled quite well. This approach is applicable to both Fraunhofer and Fresnel diffraction.

### 4.1.4 Modeling diffraction in a practical example

#### 4.1.4.1 GERB linear-array cavity detector

A project that has recently been the topic of much research in the Thermal Radiation Group involves a thermal radiation detector originally designed for GERB (Geostationary Earth Radiation Budget) [Mahan and Langley, 1996; Weckmann, 1997; Mahan *et al.*,

1998; Sánchez, 1998; Sorensen, 1998]. This detector consists of a linear-array detector housed within the wedge-shaped, mirrored cavity shown in Figure 4.6. Radiant energy from an Earth scene enters the cavity through a 60 μm wide slit. The detector is used to measure the arriving radiation in the wavelength interval between from 0.32 and 40 μm. This represents a case in which neglecting diffraction effects in the radiative model may lead to highly erroneous results.

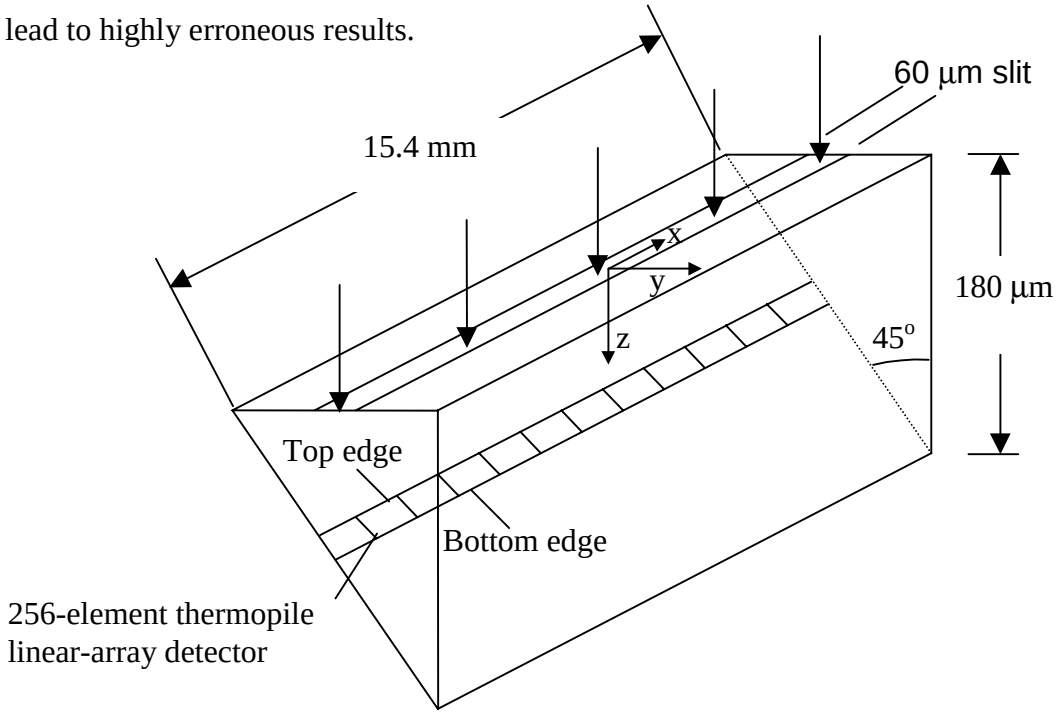


**Figure 4.6** Cavity detector developed by members of the Thermal Radiation Group.

The first step in assessing diffraction effects in the cavity detector involves determining the regime into which the occurring diffraction falls. We imagine an xy plane passing through the thermopile detector along its top edge, and use $\Delta\xi$ to determine the diffraction regime at this plane. We see that when the entering wavelength ($\lambda$) is 0.4 μm, $\Delta\xi$ = 17.3. Likewise, when $\lambda$=4.0 μm, $\Delta\xi$ = 5.5 and when $\lambda$=40 μm, $\Delta\xi$ = 1.7. Since $\Delta\xi$ >1.0 over the total range of wavelengths to be measured, diffraction within the cavity will always occur in the Fresnel region. Note that if we were to study diffraction on an xy plane passing through the bottom edge of the detector, Fresnel diffraction would still prevail over the measured wavelengths. Figure 4.7 illustrates the changing diffraction

pattern which will occur on the linear-array detector as radiant energy of three wavelengths enters the GERB cavity detector.

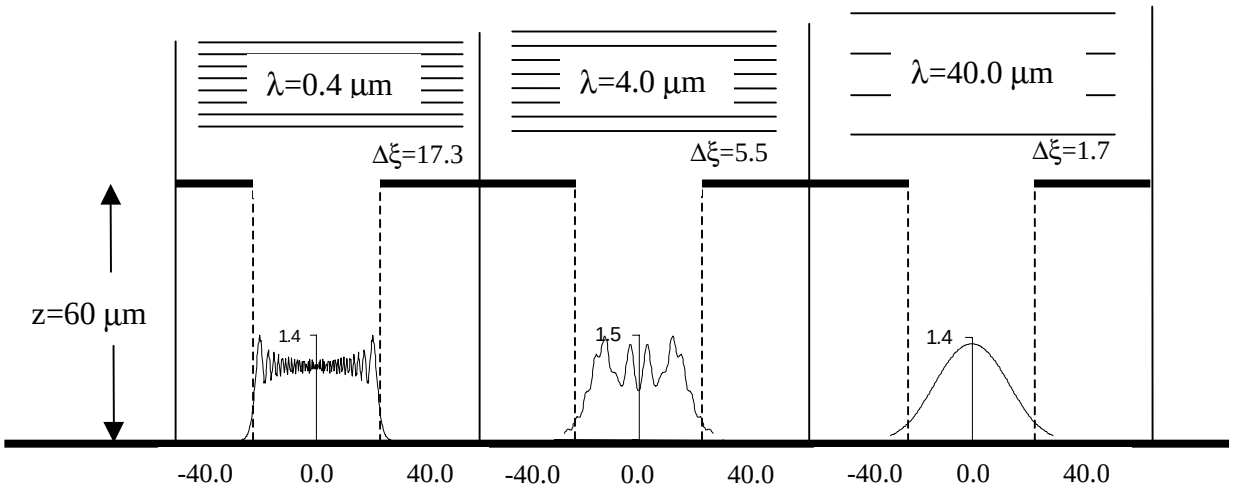


All slit widths = 60 μm

**Figure 4.7** Diffraction patterns expected at the top edge of the linear-array detector over the range of wavelengths of interest.

#### 4.1.4.2 Application of the statistical approach

The statistical approach was applied to model the diffraction of energy as it enters the GERB detector geometry. A radiative model of the GERB cavity detector which ignores diffraction effects already exists, so the effort reported here serves as a final step in the development of a complete radiative model.

The diffraction patterns obtained from the application of the statistical approach are compared to the closed-form analytical diffraction patterns in order to validate the use of the statistical method. This is also a study of an intermediate step within the statistical method. Recall that as an energy bundle enters a slit aperture, the distances from the point of entry to each edge, $\delta_1$ and $\delta_2$, are calculated. It was previously stated that we take the unknown in the entering energy bundle's position as $\delta$. We must establish which $\delta$ is to be used; that is, we must decide which edge is assumed to diffract the entering energy bundle when the slit is on the order of the wavelength of the entering energy. In cases such as the aperture of the cavity detector in Figure 4.6, which is essentially an infinite slit, it is expected that both edges should affect the momentum of the entering

energy bundle in the same direction (in the present case, the y direction). Neither of the two references cited address this situation, so four possible approaches were tested.

#### 4.1.4.3 Four methods of application of the statistical model

We have developed four methods for using the statistical model to describe diffraction. The first method involves summing the angles of diffraction due to both edges of the slit as they influence a single ray. As a ray enters, the angle of diffraction due to each edge is determined using equation 4.21, one independent of the other, and the two diffraction angles are algebraically summed to give the final diffraction angle of the entering ray.

The second method involves splitting the rays as they enter through the aperture. As a single ray enters, this single ray becomes two rays. One ray is diffracted by the first edge, located $\delta_1$ from the point of entry. The other ray is diffracted by the opposite edge, $\delta_2$ from the point of entry.

The third method involves allowing the side that is closest to the point of entry to diffract the entering ray, ignoring the other side.

The final method involves defining the angle of diffraction of an entering ray as the angle at which the ray is diffracted due to the influence of the edge that is furthest from the point of entry, ignoring the closest edge.

All four of these approaches were implemented for five different cases involving the GERB cavity detector of Figure 4.6. The angle of approach $\phi_i$ (illustrated in Figure 4.3) was zero for all cases studied. These cases involved radiation entering at wavelengths of 0.4, 4.0, 40.0, 100.0, and 160.0 μm; corresponding to values of $\Delta\xi$ of 17.3, 5.5, 1.7, 1.1, and 0.86, respectively. Note that the cavity detector is not intended to measure wavelengths beyond 40.0 μm. Diffraction was studied at 100 and 160 μm in order to test the statistical method in both the Fresnel and Fraunhofer regions, as well as in the transition region. The FORTRAN code used to conduct this study is provided in Appendix A.

#### 4.1.4.4 Results

Figures 4.8 through 4.12 provide the results of the study described in Section 4.1.4.3. Figure 4.8 involves modeling diffraction in the extremely near-field. This case approximates the diffraction situation that occurs in the GERB cavity-detector when used to measure radiation at the shortest measured wavelength of 0.32 μm. In this case, any of the four methods yields reasonable results. However, results from the summing angles, splitting rays, and closest side approaches approximate the analytical solution particularly well and are practically identical. According to the previously described criterion by Wyatt [1987], this is the only configuration for which the ideal ray approximation would be appropriate. Figure 4.9 also involves diffraction in the very near-field. In this case both the summing angles and the closest side approach yield the best results. Figure 4.10 presents the results from modeling diffraction in the barely near-field, and again the summing angles and closest side approaches work the best. This case models the diffraction situation that occurs in the GERB cavity-detector when used to measure radiation at the longest measured wavelength of 40 μm. Figure 4.11 involves modeling diffraction in the transition region. In this case the results obtained from the summing angles approach are superior to those obtained from application of all of the other three cases. Finally, Figure 4.12 involves diffraction in the far-field. In this case, either the summing angles or the closest side approach works reasonably well.

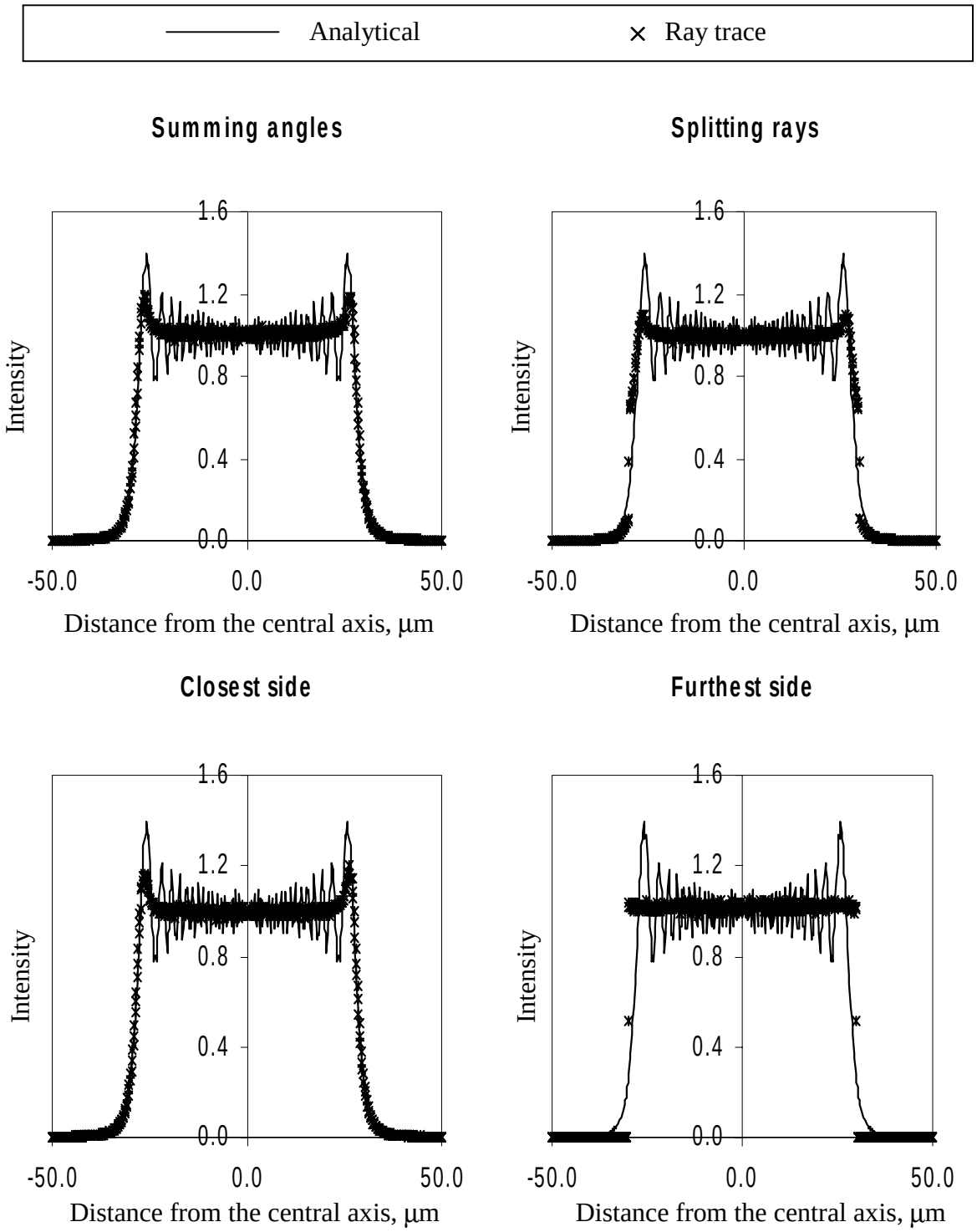


**Figure 4.8** Comparison between the results using all four methods of implementing the statistical approach to diffraction, and the closed-form analytical description of the diffraction of radiation entering the cavity detector when the entering wavelength is 0.4 μm, the slit width is 60 μm, and the distance to the screen is 60 μm.

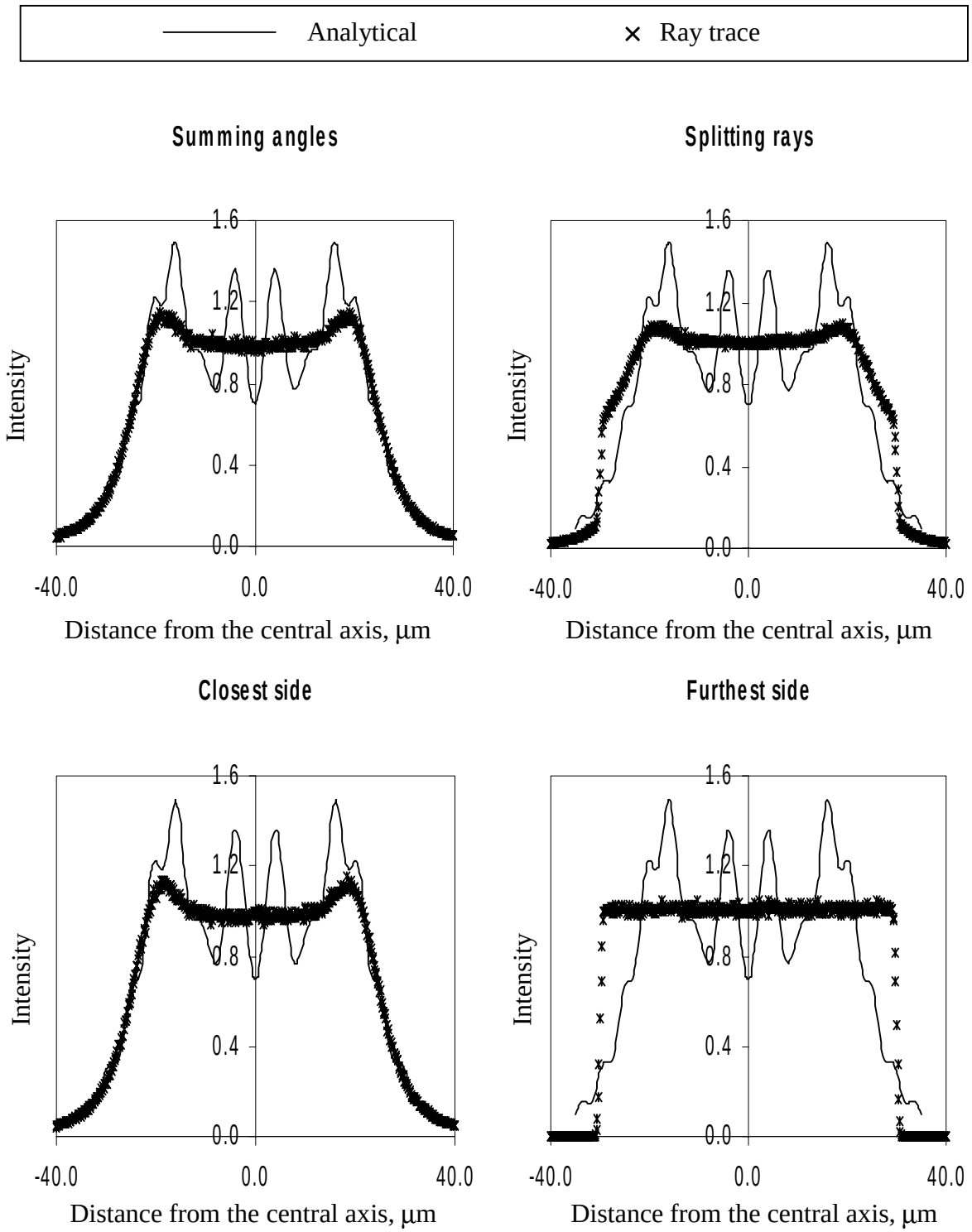


**Figure 4.9** Comparison between the results using all four methods of implementing the statistical approach to diffraction, and the closed-form analytical description of the diffraction of radiation entering the cavity detector when the entering wavelength is 4.0 μm, the slit width is 60 μm, and the distance to the screen is 60 μm.

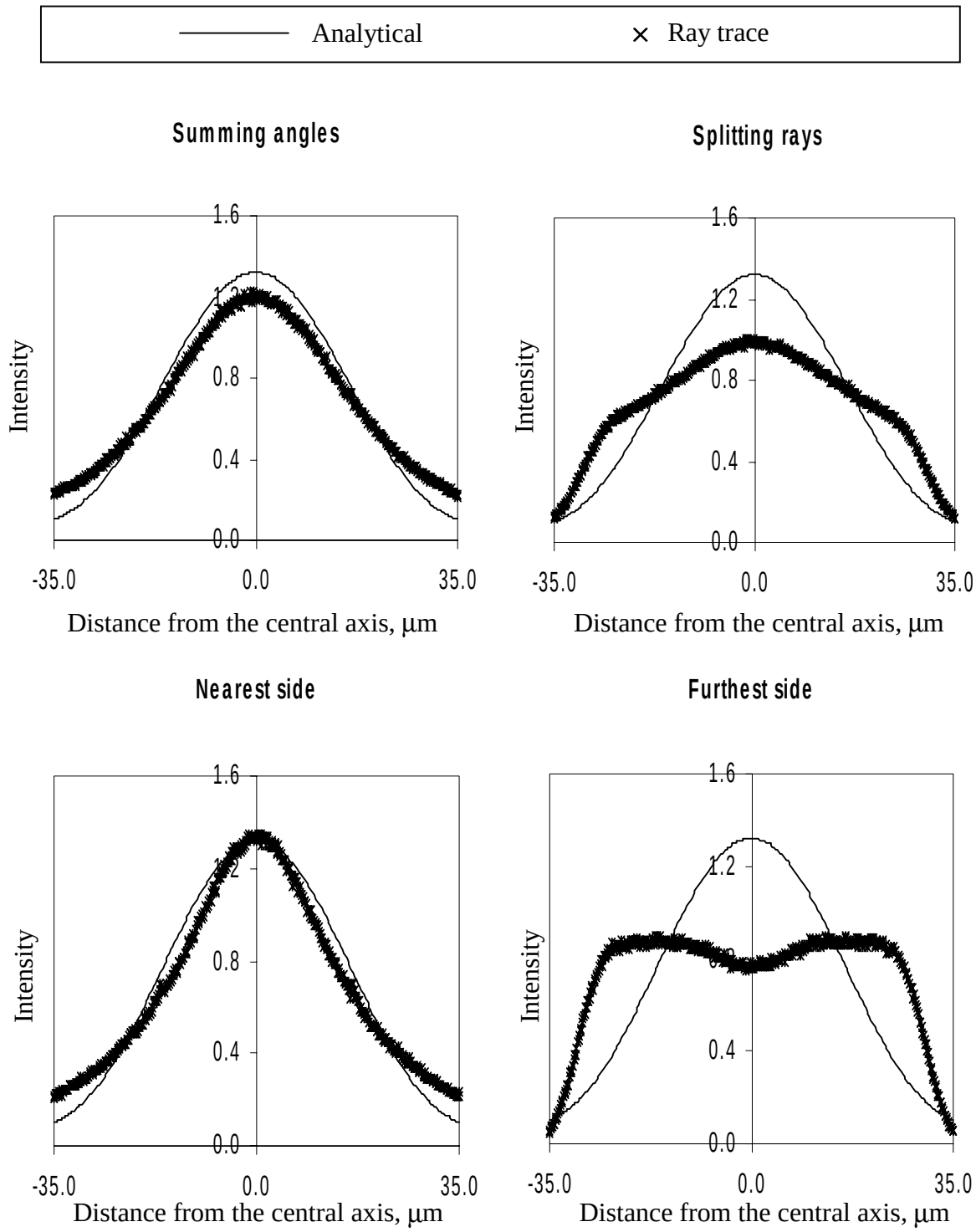


**Figure 4.10** Comparison between the results using all four methods of implementing the statistical approach to diffraction, and the closed-form analytical description of the diffraction of radiation entering the cavity detector when the entering wavelength is 40 μm, the slit width is 60 μm, and the distance to the screen is 60 μm.

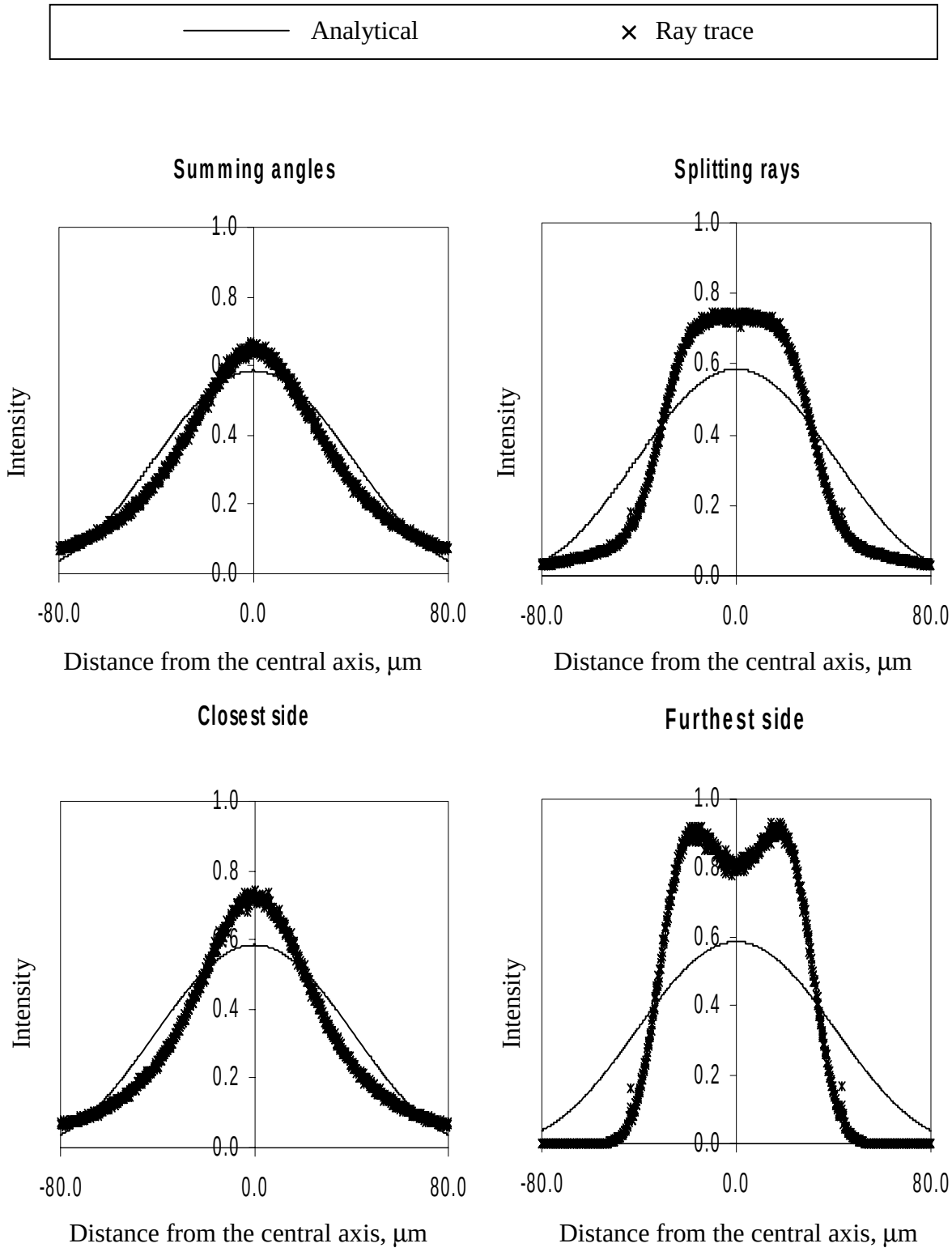


**Figure 4.11** Comparison between the results using all four methods of implementing the statistical approach to diffraction, and the closed-form analytical description of the diffraction of radiation entering the cavity detector when the entering wavelength is 100.0 μm, the slit width is 60 μm, and the distance to the screen is 60 μm.

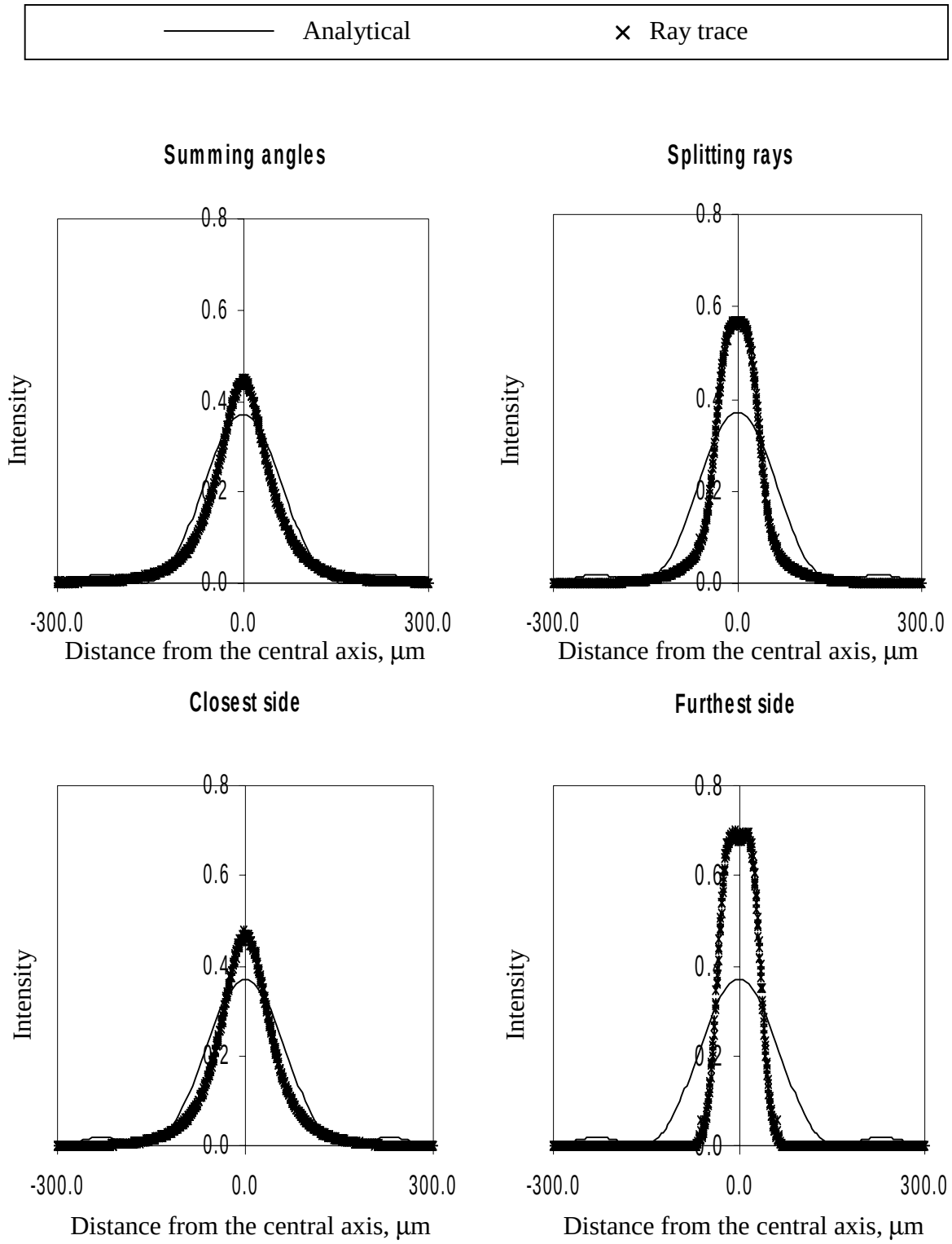


**Figure 4.12** Comparison between the results using all four methods of implementing the statistical approach to diffraction, and the closed-form analytical description of the diffraction of radiation entering the cavity detector when the entering wavelength is 160.0 μm, the slit width is 60 μm, and the distance to the screen is 60 μm.

### 4.1.5 Conclusions: Method of choice in application of statistical model

Results in Figures 4.8 through 4.12 show that the summing angles approach consistently yields good results, while the other three methods only yield acceptable results for certain cases. The results obtained while using the summing angles approach serve as validation of the statistical approach to the numerical modeling of diffraction.

## 4.2 Background for understanding diffraction Model 2

This presentation serves to provide an understanding of the nature of diffraction, and as background for understanding the second diffraction model. It borrows heavily from the presentation of Fraunhofer diffraction by an infinite slit by Serway [1994].

The first step in the determination of a diffraction pattern resulting from an infinite slit involves dividing the slit into a large number (n) of zones of width ($\Delta y$) where $\Delta y = a/n$, as illustrated in Figure 4.13.

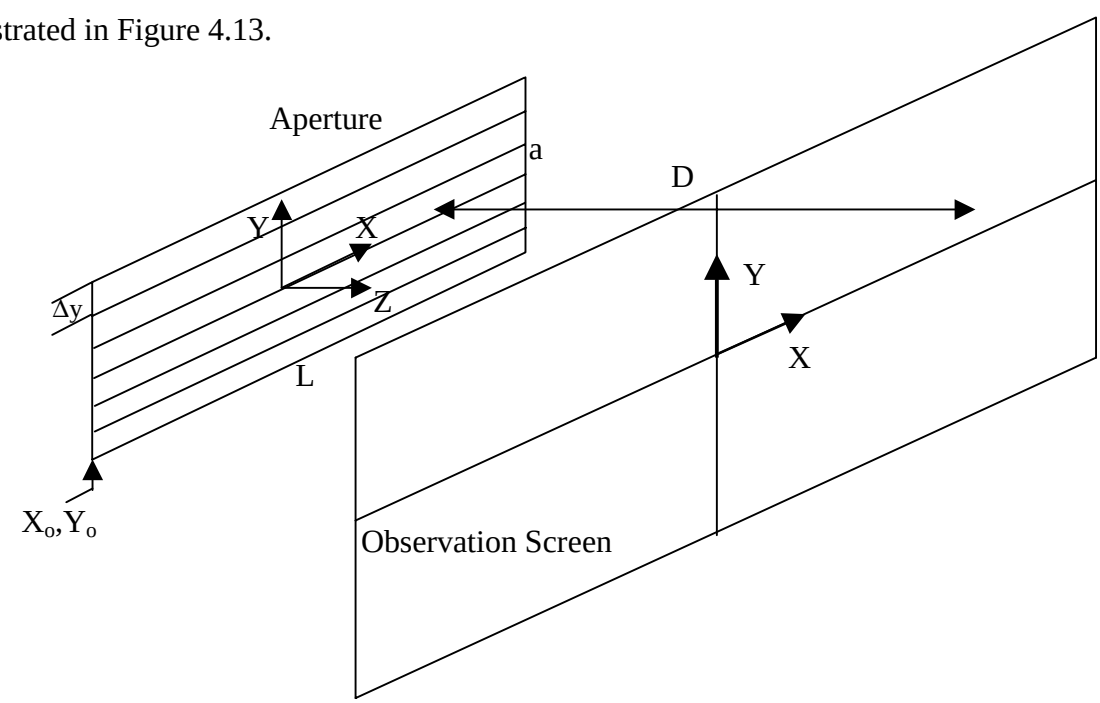


**Figure 4.13** Illustration of division of aperture into zones.

Each zone is to serve as a source of coherent radiation such that each contributes an incremental electric field amplitude, $\Delta E$, at any point on the observation screen. If this

approach were modeled in a ray-trace environment, instead of treating the most probable path for an entering energy bundle as straight ahead with a spread of paths following a normal distribution as in the statistical method, this method would treat each as having an equal probability of going in any direction. If a sufficient number of energy bundles were directed into the aperture at a given zone, the result would be an even distribution over the entire observation screen due to that zone.

Diffraction occurs because adjacent areas on an aperture all behave as independent sources. The energy leaving a given point on the aperture and arriving at a given point P on an observation screen will differ in phase from energy arriving to the same point P from another point on the aperture. The difference in path length, $\delta$, of rays coming from adjacent zones and arriving at the same point on an observation screen can be determined. This difference in path length is indicative of the difference in phase, since the phase of a ray is proportional to the distance it travels. Suppose that an infinite slit of width a is divided into two halves, as pictured in Figure 4.14.

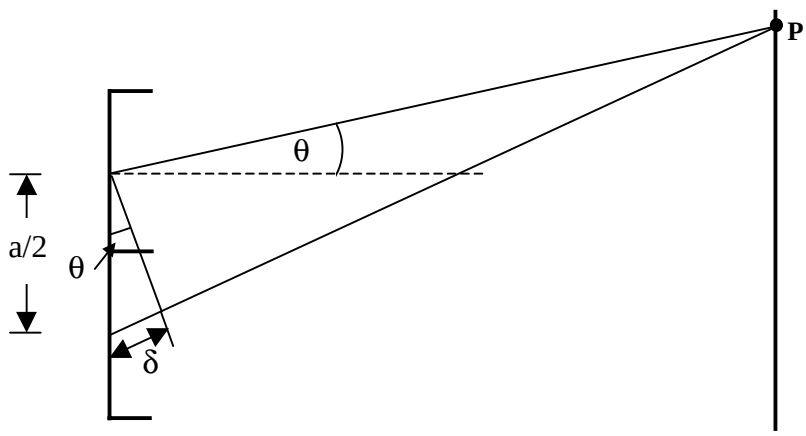


**Figure 4.14** Illustration of the determination of the difference in path length traveled by rays entering from different halves of an aperture.

The difference in path length between waves entering the two halves is given by

$$\delta = \frac{a}{2}\sin\theta\,. \tag{4.23}$$

In general, if a slit aperture is divided into n parts, the difference in path length between adjacent areas is given by

$$\delta = \frac{a}{n} \sin\theta . \tag{4.24}$$

Since the width ($\Delta y$) of the strips into which the aperture is divided is given by a/n,

$$\delta = \Delta y \sin\theta . \tag{4.25}$$

The incremental electric field amplitudes between adjacent zones are out of phase with one another by the amount $\Delta B$, given by

$$\Delta B = \frac{2\pi\delta}{\lambda}, \tag{4.26}$$

where $\lambda$ is the wavelength of the entering radiation, and $\delta$ is the difference in path length traveled by energy bundles leaving adjacent areas and arriving at the same point on the screen. Using phasor diagrams to determine the intensity at a given point, the total electric field is obtained by summing the contributions from all zones at a given point on the observation screen. The chord length, $E_{\theta P}$, is taken to be the amplitude of the electric field at P. Figure 4.15 (b) illustrates the addition of phasors for an infinite slit divided into four areas, shown in 4.15 (a). When the number of divisions on the aperture goes to infinity, the phasor diagrams become smooth curves, as illustrated in 4.15 (c).

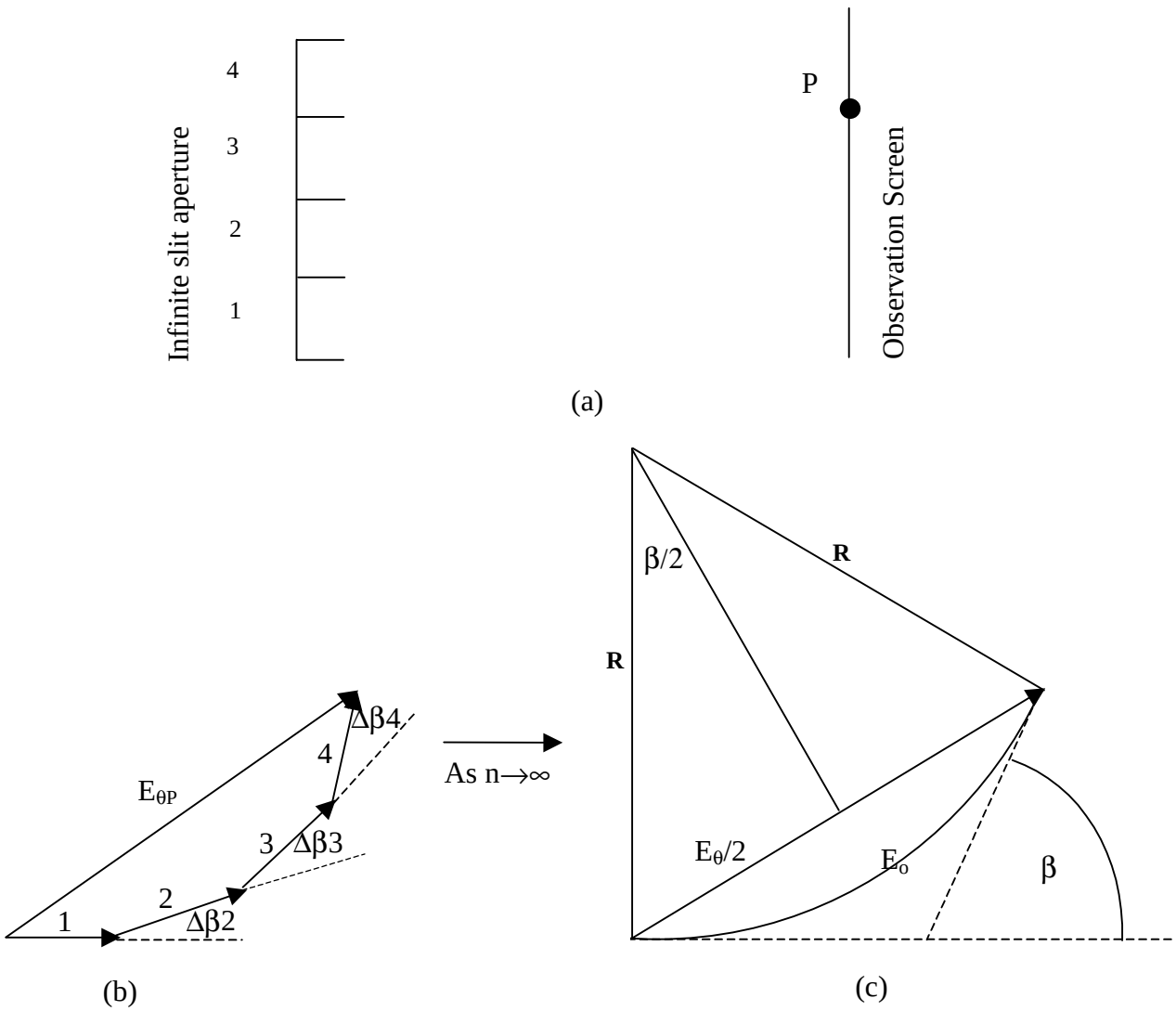


**Figure 4.15** Determination of the amplitude of the electromagnetic field at a point on an observation screen placed in front of an infinite slit aperture. (a) Illustration of slit division, (b) phasor diagram construction, and (c) smooth curve that the phasor diagram becomes as the number of slit divisions goes to infinity.

Taking the arc length to be $E_o$, R to be the radius of curvature, and the total phase angle from the top to the bottom of the aperture to be β, simple geometric relations show that

$$\sin\frac{\beta}{2} = \frac{E_\theta/2}{R} \tag{4.27}$$

Substituting the fact that the arc length, $E_o$, is given by Rβ yields

$$E_\theta = E_o\left[\frac{\sin(\beta/2)}{(\beta/2)}\right]. \tag{4.28}$$

Since intensity is proportional to the square of the electric field, we can then write

$$I_\theta = I_{max}\left[\frac{\sin(\beta/2)}{(\beta/2)}\right]^2, \tag{4.29}$$

where $I_{max}$ is the intensity of the central maximum. Because we are discussing the entire slit, $\Delta y = a$, thus $\delta = a \sin\theta$. Substituting into equation 4.26, $\beta$ in this case is given by

$$\beta = \frac{2\pi a \sin\theta}{\lambda}. \tag{4.30}$$

## 4.3 Model 2: Application of the modified Huygens-Fresnel principle

### 4.3.1 Basic description of Model 2

The second model proposed for use in the modeling of diffraction in the Monte-Carlo ray-trace environment is based on concepts presented in Section 4.2. It involves firing rays into an aperture, and modeling each point of ray entry as a source itself. The original plan for this approach was to model the point of entry of a ray as a source as defined by the Huygens-Fresnel principle, whereby the diffracted ray would have equal probability of going in any direction and each ray would carry with it an amplitude of unity. The distance traveled by the emitted ray before being intercepted by an observation screen was to be determined, and the phase assigned to this ray would be proportional to its length of travel. After many rays had been traced, the resulting intensity distribution was to be determined using a method that will be described shortly. The results obtained from the application of this approach did not agree with theory, as the secondary peaks were too high relative to the central maxima. A modified approach was then implemented in which the point of entry is modeled as a source which emits a ray in any forward direction. The amplitude of the optical field at any point on the observation screen is taken to be the superposition of all the rays arriving to that point (considering their amplitudes and relative phases). This approach is different from the initial approach in that all rays do not carry the same amplitude of unity. Instead, the

magnitude of each ray is determined by an obliquity factor which is a function of the angle of ray diffraction.

### 4.3.2 The obliquity factor

The obliquity factor serves to properly model the variations in amplitude with angle over the surface of the secondary wavelets emanating from a source point, modeled incorrectly by the Huygens-Fresnel principle [Hecht and Zajac, 1974]. Kirchoff proposed that the obliquity factor, K, be given by

$$K(\phi_i, \phi_d) \cong \frac{1}{2}(\cos\phi_i + \cos\phi_d)\,, \tag{4.31}$$

where $\phi_i$ is the angle of incident radiation and $\phi_d$ is the angle of diffraction, as illustrated in Figure 4.3 [Mayes and Melton, 1994]. Later modified by Rayleigh and Sommerfeld, and then by Miller, the suggested obliquity factor became

$$K(\phi_d) = \cos(\phi_d)\,. \tag{4.32}$$

For the present purposes, use of either of these factors provides comparable results. Figure 4.16 shows the weighting to be placed on an diffracted ray as a function of diffraction angle when the incident energy approaches normal to the slit, as suggested by Huygens, Kirchoff, Rayleigh and Sommerfeld and Miller.

Figure 4.17 demonstrates how a source point of radiant entry would be modeled if we were to apply the Huygens-Fresnel principle alone. When weighted by the Rayleigh/Sommerfeld obliquity factor, the entry point is modeled as illustrated in Figure 4.18.

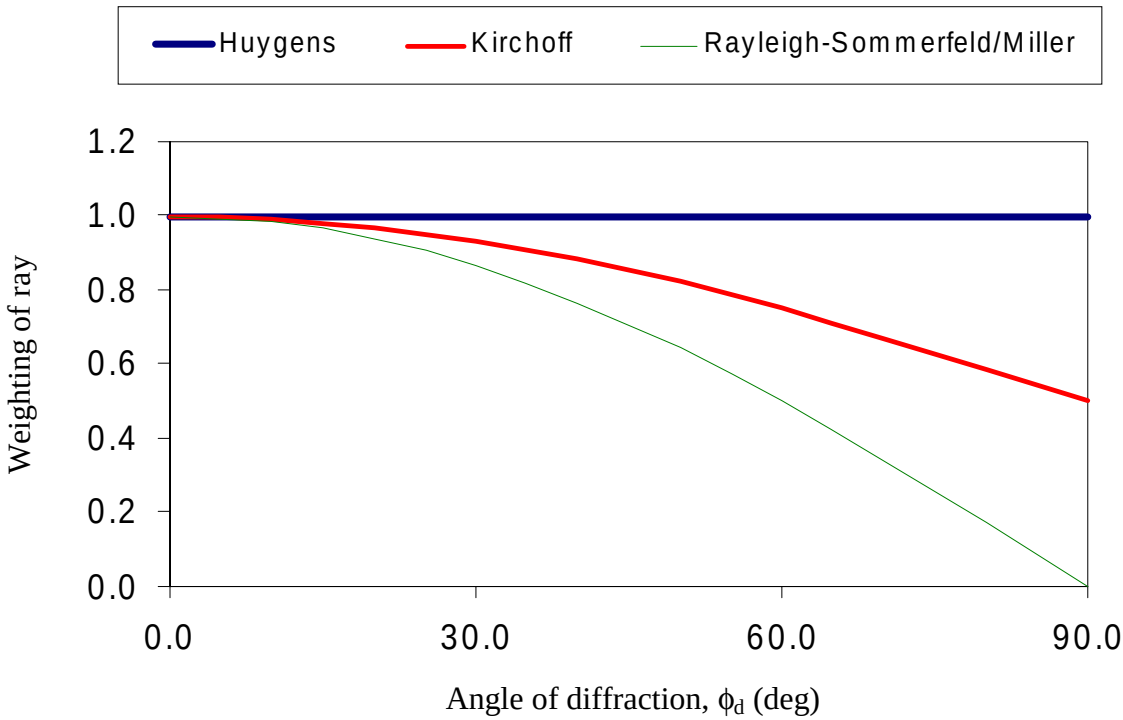


**Figure 4.16** Weighting to be placed on rays when using two different obliquity factors, or none at all.

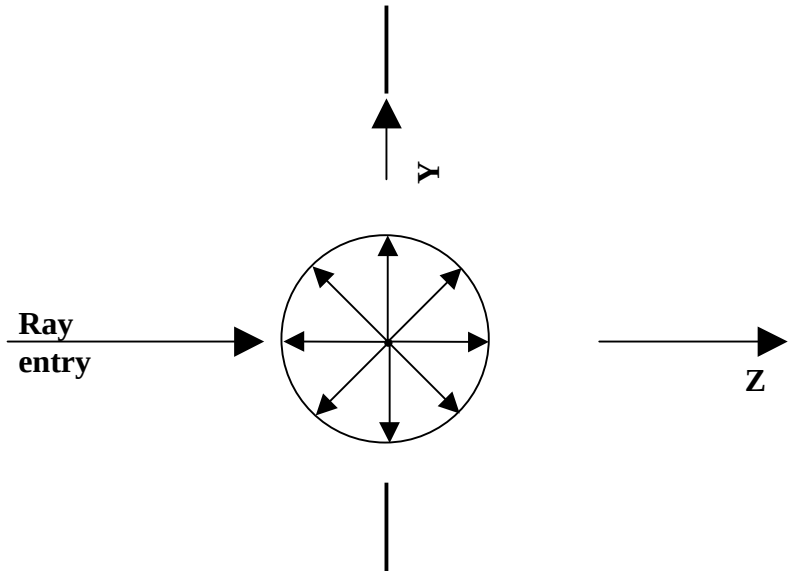


**Figure 4.17** Model of a point source of rays entering a slit when employing the Huygens-Fresnel principle with no obliquity factor.

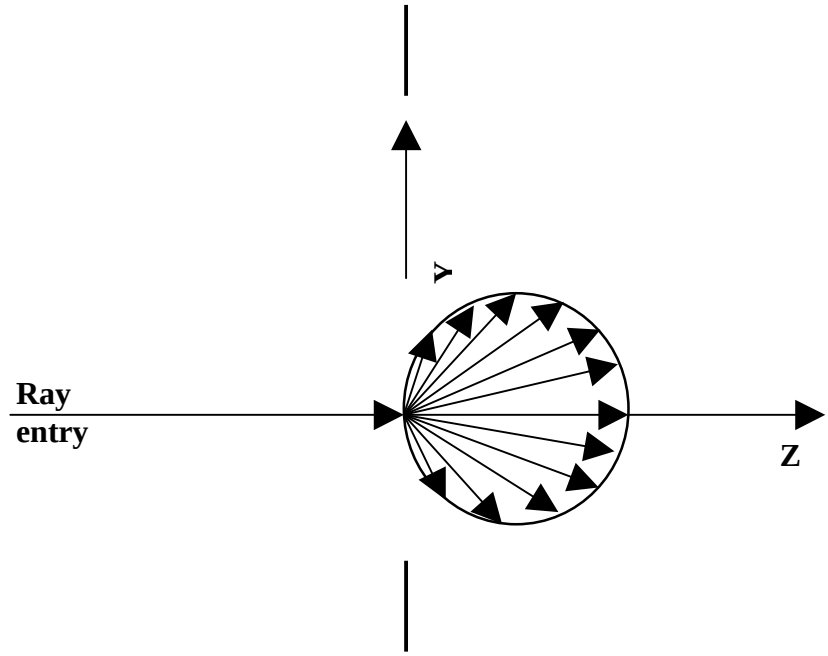


**Figure 4.18** Model of a point source of rays entering a slit when employing the Huygens-Fresnel principle with the Rayleigh/Sommerfeld obliquity factor applied.

### 4.3.3 Application of Model 2

The implementation of Model 2 in the Monte-Carlo ray-trace environment for the prediction of the far-field diffraction pattern involves firing energy bundles uniformly and randomly across the aperture towards the observation screen which is divided into a large number of bins, as in the statistical model. In this case, however, the angle of diffraction is chosen so that all angles are equally probable (diffusely scattered) rather than following a normal distribution. The length of the path that each energy bundle travels and the angle at which it is diffracted are substituted into a modified form of equations 4.26 and 4.29. Taking the amplitude of the electric field of a given energy bundle to be

$$E_{eb} = K(\phi_i, \phi_d)\frac{\mathrm{Sin}(\beta)}{\beta}, \tag{4.33}$$

where

$\beta = 2\ell\frac{\pi}{\lambda}$ and $\ell$ is the path length. After a large number of rays has been fired (e.g. one million), the final intensity in a given bin on the observation screen is the square of the

sum of all of these electric fields due to energy bundles arriving at this bin from all parts of the aperture, given by

$$I_{bin} = \left[\sum E_{eb}(bin)\right]^2 . \tag{4.34}$$

Determining $I_{bin}$ for all bins on the observation screen and dividing by the maximum intensity arriving in any of the bins provides the normalized intensity along the observation screen. This technique was tested on two configurations, chosen so that the diffraction would be in the Fraunhofer diffraction regime.

### 4.3.4 Results from the application of Model 2

The results from the application of Model 2 are presented as normalized intensity compared with the normalized closed-form analytical solution. Figure 4.19 presents the results from application of this approach to an infinite, 0.3-mm-wide slit with energy entering at the wavelength of 0.58 μm, and an aperture-to-screen distance of 2 m.

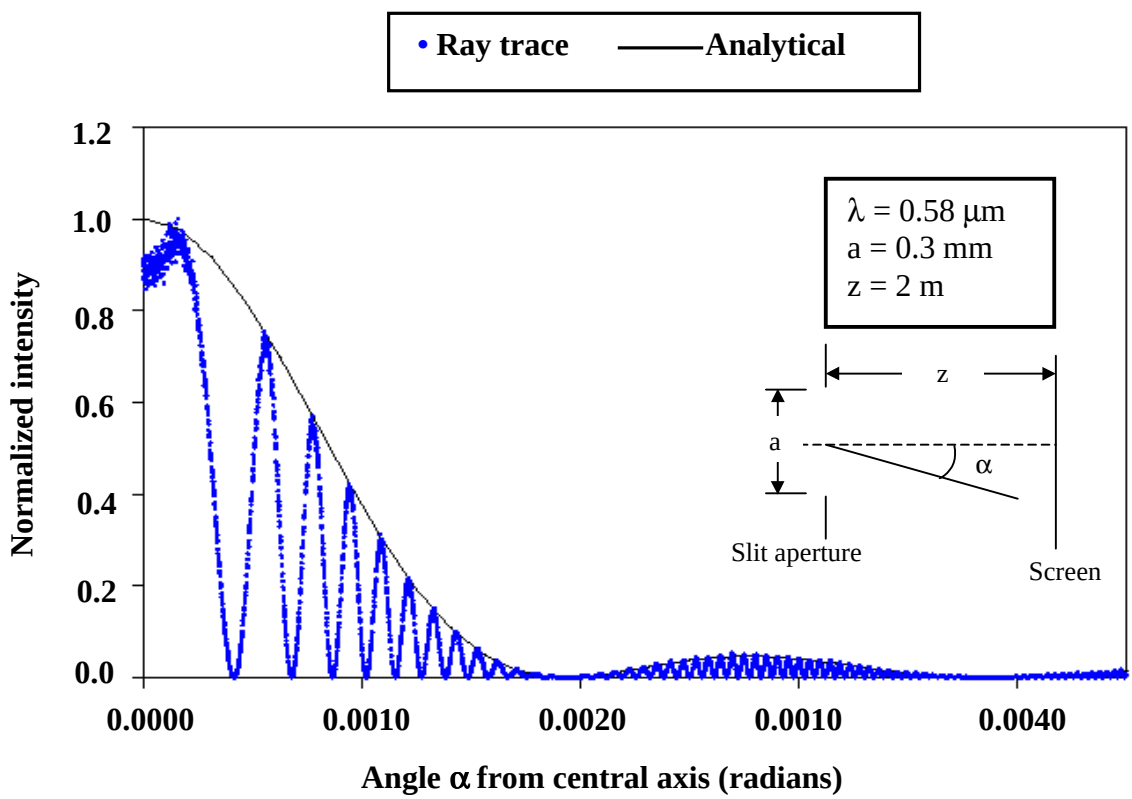


**Figure 4.19** Comparison of results from application of modified Huygens-Fresnel principle and analytical solution for far-field diffraction from an infinite slit.

Note that this approach produces a pattern with high-frequency oscillations in intensity, whose peaks lie within an envelope that matches the closed-form analytical solution quite well.

It is interesting to study the application of Model 2 to other aperture shapes, such as a circular aperture. A circular observation screen divided into bins consisting of equal-area rings is placed behind this aperture, and the same procedure is followed to obtain a plot of intensity with angle from the central axis. The case studied involved a circular aperture 0.2 mm in diameter with entering energy of wavelength 9 μm, and aperture to observation screen distance of 16 m.

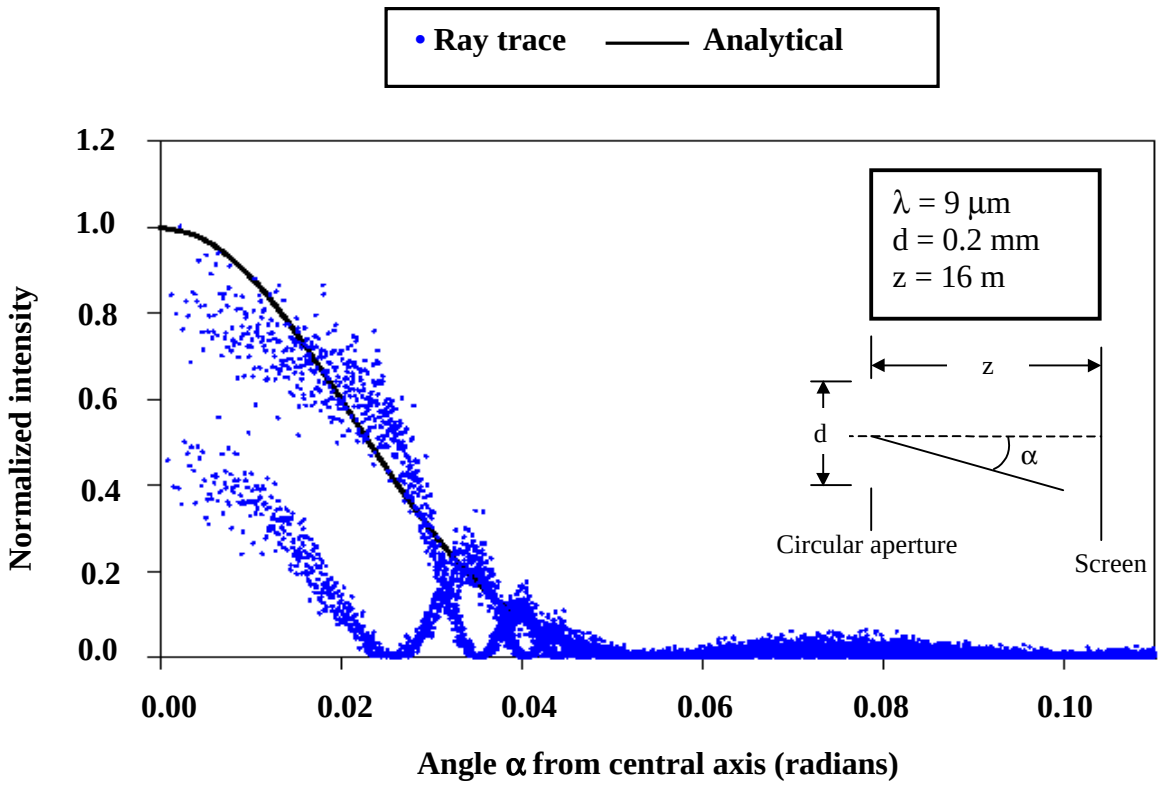


**Figure 4.20** Comparison of results from application of modified Huygens-Fresnel principle and analytical solution for far-field diffraction from a circular aperture.

The resulting intensity pattern shown in Figure 4.20, when compared to the analytical solution, is more difficult to interpret than that for the infinite slit. For this case, two oscillating patterns, or orders, occur which together form an envelope that approximately matches the analytical solution. The oscillating intensity patterns seen in both cases occur for reasons that are not clear. For the case of the slit, the resulting pattern is similar to that formed by radiation passing through multiple closely-spaced slits [Hecht and Zajac, 1974]. The agreement between the diffraction predicted by this model, and the closed-form analytical solution will occur in certain cases when the Fraunhofer condition applies, described in Sections 4.3.5 through 4.3.7. Otherwise, the simplifying assumptions break down, and we can no longer expect good results from this application of the modified Huygens-Fresnel principle [Hecht and Zajac, 1974]. The FORTRAN code used to generate these results is provided in Appendix B.

### 4.3.5 Limitations of the Huygens-Fresnel principle and of Model 2

Because Model 2 is based upon the modified Huygens-Fresnel principle, it is important to understand the limitations of this principle. As stated by Hecht and Zajac [1974], in cases in which the aperture is very large, and the point of observation is far away, the Huygens-Fresnel principle should, and does, work very well. However, for cases involving a very small aperture, or when the point of observation is in the vicinity of the aperture, deviation from the behavior predicted by the Huygens-Fresnel principle should be appreciable. Here, the size of the aperture refers to the aperture dimensions relative to the wavelength of the entering radiation. These limitations imply that Model 2 may properly model diffraction only for configurations where $\Delta\xi < 1.0$, and where the aperture width-to-wavelength ratio ($a/\lambda$) exceeds some minimum value. In order to investigate these limitations, several cases were studied in which the value of $\Delta\xi$ and the aperture width were held constant, while the ratio of $a/\lambda$ was varied. These cases were studied by comparing the closed-form analytical solution of the diffraction pattern with the results predicted by Model 2.

The case study involved modeling diffraction by an infinite, 60 μm-wide slit. The wavelength of the entering radiation and the aperture-to-observation screen distance were

varied so that $\Delta\xi$ was a constant 0.4. Five cases were studied, whereby $a/\lambda$ was assigned the values of 4.0, 1.5, 1.0, 0.5, and 0.25. The results from this study are provided in Section 4.3.6.

### 4.3.6 Results from case study

Model 2-predicted results shown in Figure 4.21 agree well with the analytical solution (the envelope containing the peaks of the oscillating pattern predicted by Model 2 approximately match the closed-form analytical solution). For this case, the entering wavelength is four times smaller than the aperture width and the observation points are far from the aperture; as expected, the Huygens-Fresnel principle works well. Figure 4.22 demonstrates the declining performance of the Huygens-Fresnel principle as the wavelength of the entering radiation approaches the width of the slit. Here the central maxima is outlined by the peaks of the oscillating pattern predicted by Model 2, but the secondary fringes are lost entirely. The results shown in Figure 4.23 are for the case in which the entering radiation is of the wavelength equal to the slit width. These results are beginning to lose the ability to predict even the shape of the central maxima. As the entering wavelength is made larger than the slit width, Model 2 produces highly erroneous results, as illustrated in Figures 4.24 and 4.25.

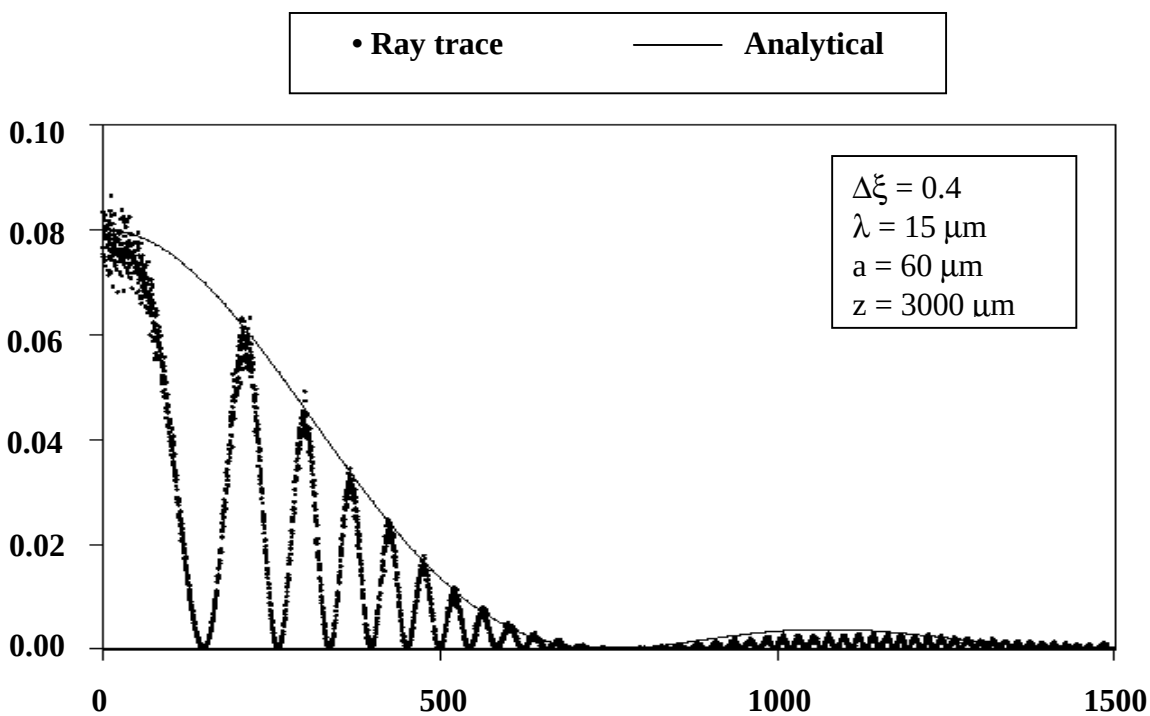


**Figure 4.21** Comparison of results from application of modified Huygens-Fresnel principle and analytical solution for far-field diffraction from an infinite slit aperture for which $\Delta\xi = 0.4$ and $a/\lambda = 4.0$.

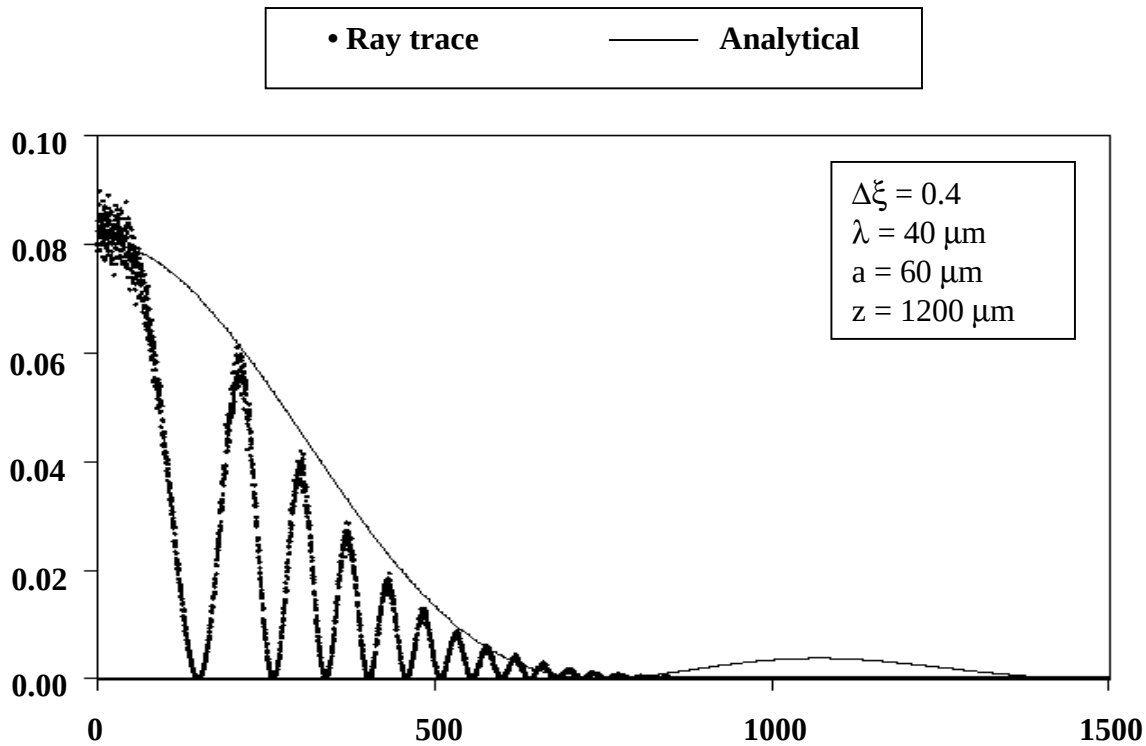


**Figure 4.22** Comparison of results from application of modified Huygens-Fresnel principle and analytical solution for far-field diffraction from an infinite slit aperture for which $\Delta\xi = 0.4$ and $a/\lambda = 1.5$.

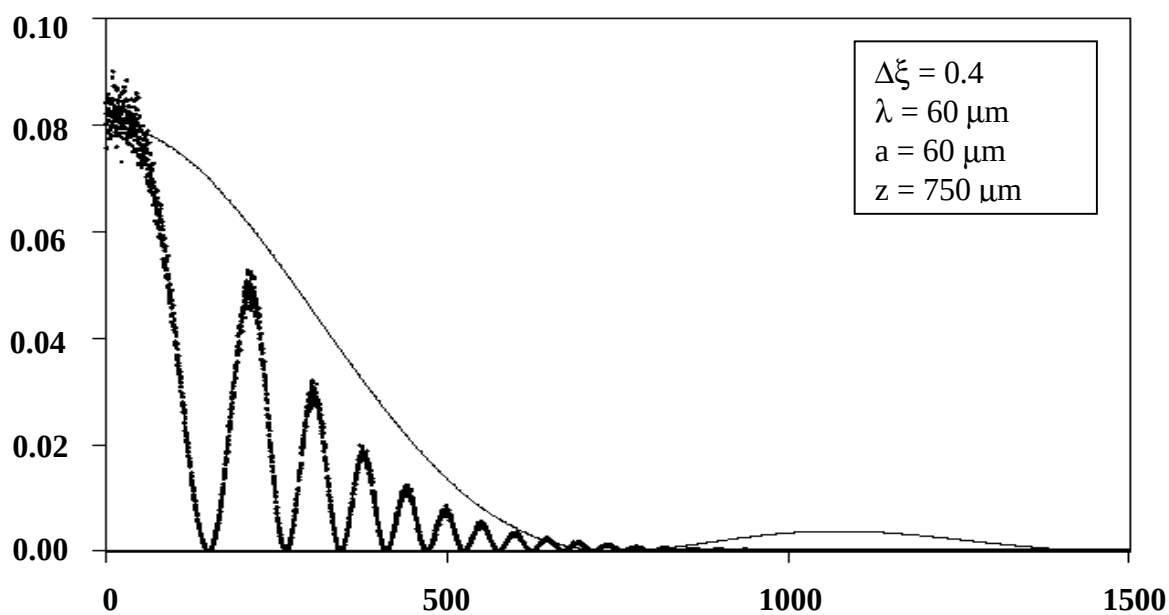


**Figure 4.23** Comparison of results from application of modified Huygens-Fresnel principle and analytical solution for far-field diffraction from an infinite slit aperture for which $\Delta\xi = 0.4$ and $a/\lambda = 1.0$

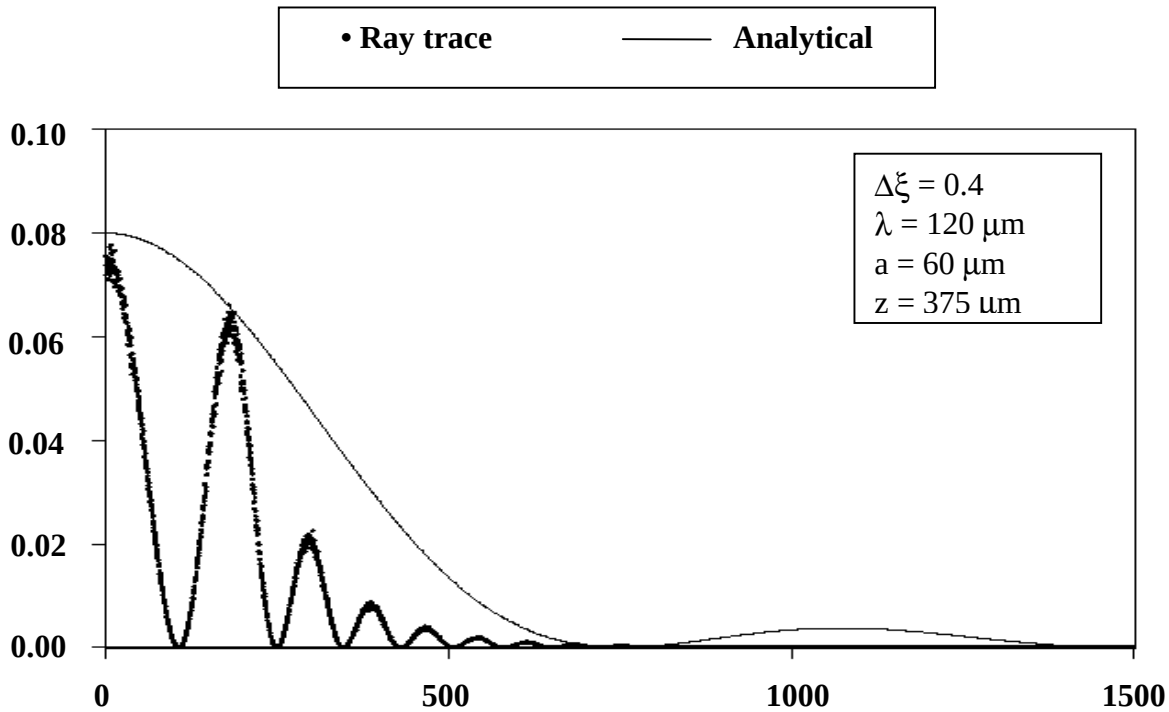


**Figure 4.24** Comparison of results from application of modified Huygens-Fresnel principle and analytical solution for far-field diffraction from an infinite slit aperture for which $\Delta\xi = 0.4$ and $a/\lambda = 0.5$.

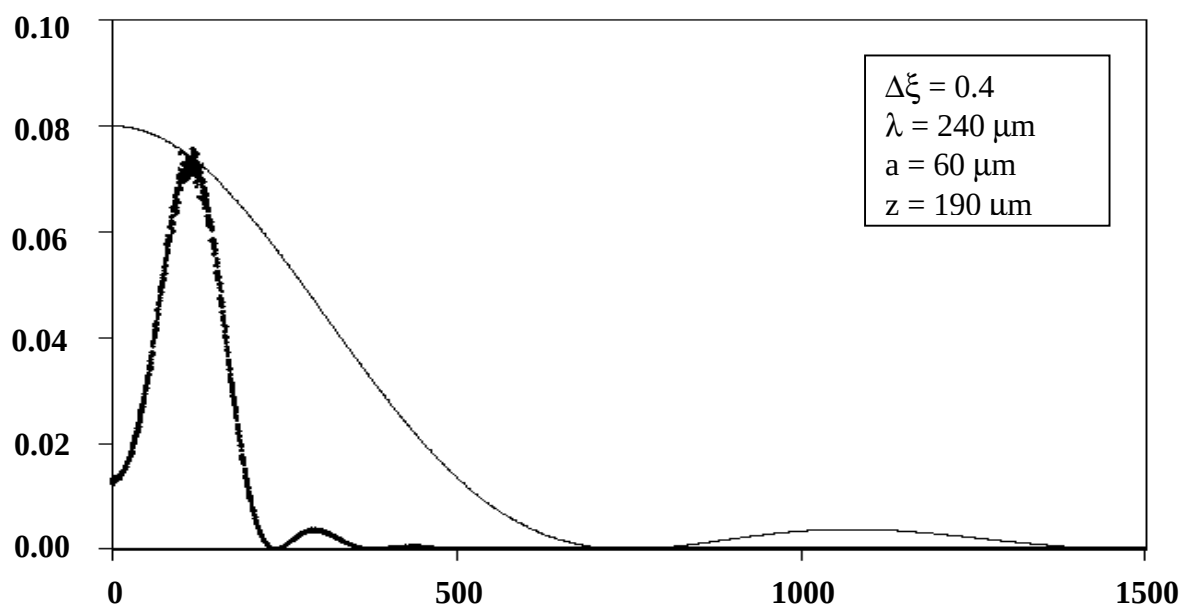


**Figure 4.25** Comparison of results from application of modified Huygens-Fresnel principle and analytical solution for far-field diffraction from an infinite slit aperture for which $\Delta\xi = 0.4$ and $a/\lambda = 0.25$.

### 4.3.7 Conclusions: Model 2

The results from the case study described in Section 4.3.6 suggest that Model 2 will approximate the diffraction pattern of radiant energy entering an aperture, including the secondary maxima only if $\Delta\xi < 1.0$, and $a/\lambda >> 1.0$. Results indicate that as long as $a/\lambda > 1.0$, application of Model 2 will not lead to highly erroneous results, but the details of the secondary fringes may be lost. However, if $a/\lambda < 1.0$, Model 2 should not be applied as its underlying principles are no longer sound.

## 4.4 Conclusions: Model 1 versus Model 2

The statistical model is the most general choice for the modeling of diffraction in a Monte-Carlo environment, as it can approximate interference patterns caused by the diffraction of energy for both near and far-field conditions. This model cannot be modified to predict the fringes about the central maxima by keeping track of phase angle ($\beta$) as is done in the second model. This impossibility is due to the requirement that all points on the aperture contribute equally to all bins on the observation screen for the formation of an interference pattern. In other words, the number of arriving rays (coming from any randomly located point on the aperture) must be the same for each bin, but the resulting intensity is given by the sum of the intensity from each individual ray, weighted by its phase angle. In the statistical approach, this criterion is not met, as the distribution of energy from a given point on the aperture is not diffusely distributed, but follows a normal distribution. Model 2 can only be used with good results for a restricted set of conditions, otherwise the underlying assumptions break down and it behaves very poorly.

## 4.5 Potential future investigations of diffraction models

The model based upon the modified Huygens-Fresnel principle (Model 2), and the cause of the oscillating intensity pattern it predicts, should be further investigated. Other case studies similar to the one presented in Section 4.3.6 could be conducted to determine the generality of the conclusions in Section 4.3.7. Another unexplored aspect of the diffraction of radiant energy by an aperture involves the behavior of radiation as it approaches an aperture (prior to entry through the aperture), and the possibility of backwards diffraction. The geometric theory of diffraction described in Chapter 3.0 does

model both forward and backward diffraction of energy as it approaches an aperture, and may be capable of properly modeling this behavior. Useful future work could also involve the development of an approach to scale ray-trace results to match the analytical curve for the statistical method, as the current method involves simply scaling the results "by eye" until the area under the ray-trace curve appears to match that of the analytical curve.